PROCEEDINGS OF SCIENCE

The Wavelength-Shifting Optical Module in Application to the IceCube Neutrino Observatory

The IceCube Collaboration

(a complete list of authors can be found at the end of the proceedings)

E-mail: ypopovyc@uni-mainz.de

The Wavelength-shifting Optical Module (WOM) is a novel photosensor concept developed as part of the upcoming Upgrade for the IceCube Neutrino Observatory. It uses the technique of wavelength shifting and total internal reflection to increase the photon light yield in the UV-regime of the Cherenkov spectrum. The decoupling of the effective area from the size of light sensors enhances the signal-to-noise-ratio. Twelve WOM modules will be deployed in the IceCube Upgrade to increase the photon detection efficiency and thus enhance future low-energy analyses. The general concept can also be applied at the future IceCube-Gen2 detector, where passive light collecting extensions to the optical sensor modules locally increase the light collection efficiency. This technique would benefit the detection of supernova neutrinos or other particles with low light emissions. We report on new results in characterizing and optimizing the WOM concept, the production status of the modules to be deployed in 2025/26 as well as possible applications of the concept for IceCube-Gen2.

Corresponding authors: Yuriy Popovych[1*]

[1] *Institute for Physics, Johannes-Gutenberg Universität Mainz, D-55122 Mainz, Germany*

[*] Presenter

The 38th International Cosmic Ray Conference (ICRC2023)
26 July – 3 August, 2023
Nagoya, Japan

PoS(ICRC2023)992

1. The IceCube Neutrino Observatory

The IceCube Neutrino Observatory [1] is a large scale neutrino detector instrumenting 1 km^3 of Antarctic ice as the detection medium. It uses 10" Photo-Multiplier Tubes (PMTs) located inside 5160 deployed Digital-Optical Modules (DOMs) to detect the Cherenkov light produced by secondary particles from neutrino interactions with the ice. The 17 m vertical and 125 m horizontal spacing of the modules allows for the reconstruction of high-energy neutrino events in the energy range of O(TeV)-O(PeV). While IceCube does not have the dense instrumentation required to reconstruct individual low-energetic O(10 MeV) neutrinos from core-collapse supernovae (CCSNe), a CCSN is instead observed as an increase of the detector noise level [2]. The IceCube detector has model-independent sensitivity within the Milky Way and has some model-dependent sensitivity reaching out to the Large and Small Magellanic Clouds.
The main goal of the upcoming IceCube Upgrade [3], which will be deployed in 2025/26, is the enhancement of the detection of low-energy neutrinos and the improvement of low-energy analyses in IceCube. Using 5 m vertical and 20 m horizontal spacing as well as new multi PMT optical modules like mDOMs [4] and D-Eggs [5] IceCube's capabilities in the GeV energy range will be significantly enhanced. The calibration devices included in Upgrade modules will allow measurement of the ice properties, which is the leading systematic uncertainty in the directional reconstruction for high energy neutrinos. Further, there will be novel photo sensor concepts deployed in small numbers such as the Wavelength-Shifting-Optical Module (WOM).
The envisaged IceCube-Gen2 detector [6] will comprise in the order of 10,000 new in-ice modules increasing the detector volume by a factor of 8 resulting in a 5 times higher sensitivity for high-energy neutrinos.

2. WOM Hardware Design

Current IceCube modules are are limited to the visible region of the Cherenkov spectrum because of the pressure vessels used, while the intensity peaks in the UV-regime following an approximate $\frac{1}{\lambda^2}$ dependency [7]. In addition, the sensitivity to low-energy neutrino signals of the optical modules is constrained by the sensor noise rate which is mainly driven by the size of the photo cathode. The WOM increases the UV-sensitivity by the application of UV-sensitive paint and furthermore allows to decouple the photosensitive area of the module from the PMT photo cathode. Due to these characteristics, sensors based on wavelength-shifting technologies are well suited for the detection of low signal-to-noise ratio events such as the detection of low-energy CCSNe neutrinos. The general WOM concept is visualized in Figure 1. A transparent quartz tube is coated with wavelength-shifting (WLS) paint on the outside, absorbing and shifting UV-photons with almost 100% efficiency. The re-emitted photons are then captured inside the tube by total internal reflection with an efficiency of 41% in ice and propagate to one of the two 5" ET9390B PMTs [8] located on the top and bottom end of the cylinder. To withstand the pressure of being frozen in ice the WOM-Tube is located inside a quartz pressure vessel (length: 1200 mm, outer diameter: 173 mm, wall thickness: 14 mm). The space between WLS-tube and pressure vessel is filled with perfluoropolyether (PFPE) chosen based on its refractive index, chemical inertness and good optical transparency. The WOM concept and its hardware design was already discussed in

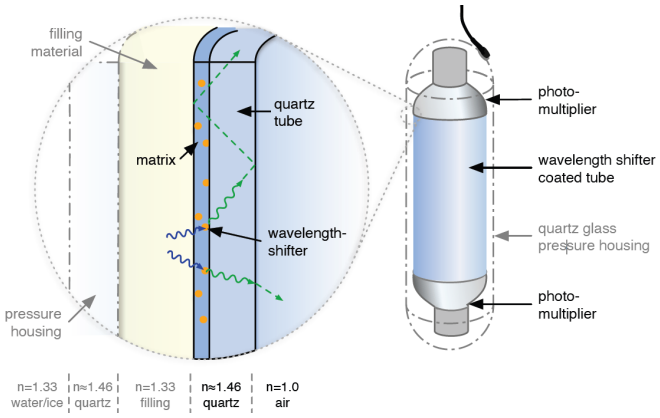

Figure 1: Working principle of the WOM. UV photons are absorbed, shifted and re-emitted by the wavelength-shifting paint on the outside of the tube.Photons re emitted below the angle of total internal reflection propagate to the PMTs at both ends of the tube.

detail in [9]. Here we report on new hardware studies regarding the WLS-paint and coating process (see section 2.1) as well as analysis of the timing of the propagated photons inside the tube (see section 2.2). Furthermore, we discuss the advantages for WOM application in the IceCube Upgrade presenting the first Upgrade WOM Prototype (see section 3). Finally, we describe the potential of this technology for IceCube-Gen2 (see section 4) and its application in supernova detection and for other experiments besides IceCube (see section 5).

2.1 WLS-Paint and Coating

The WLS-effect of our paint arises from the two dissolved wavelength-shifters Bis-MSB and p-Terphenyl. Assuming a paint layer thickness of at least 25 μm we observe a flat absorption spectrum between 250 and 400 nm with almost 100% efficiency and an emission spectrum between 400 and 600 nm. From the studies on the WLS-paint and coating in [9] we know that the resulting paint layer thickness d_0 can be affected by the coating speed U_0. A prediction can be made by the *Landau-Levich model*:

$$d_0 = 0.8 \cdot \sqrt{\frac{U_0 \cdot \eta}{\rho \cdot g}}. \tag{1}$$

This model can be verified for our case by coating quartz slides with different coating speeds and measuring the paint layer thickness by the mass difference before and after coating. The results (see Figure 2) show that we can fit our layer thicknesses and coating speeds to the Landau-Levich model and are therefore able to achieve a certain layer thickness by setting up the coating speed.

In relation to the thickness and concentration of Bis-MSB in the paint layer, the spectrum was also examined for self-absorption. For this purpose, the spectrum of a coated rod was examined as a function of the distance travelled by the light in the rod (see Figure 3). It can be seen that the spectrum has a cut off below 400 nm. In addition, a redistribution to higher wavelengths occurs with increasing distance. These effects depend on the concentration of Bis-MSB and result in wavelength-dependent absorption as well as a reduction in the effective capture rate when parts of

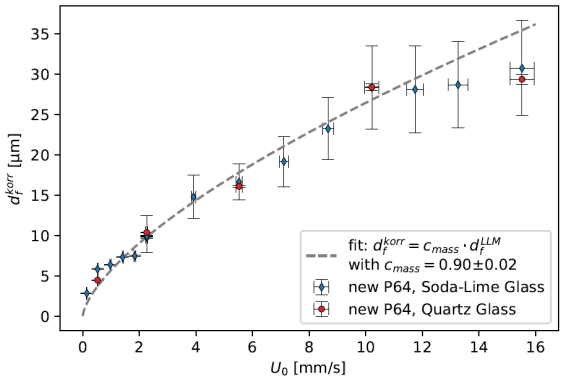

Figure 2: WLS coated slides fit to the Landau-Levich model. The real d_0 was determined by weighing the slide before and after coating. Further, one can check for a homogeneous paint layer with illumination measurement or a profilometer. The measured thickness had to be corrected due to drops dripping down from the slide during the drying process. (Taken from [10])

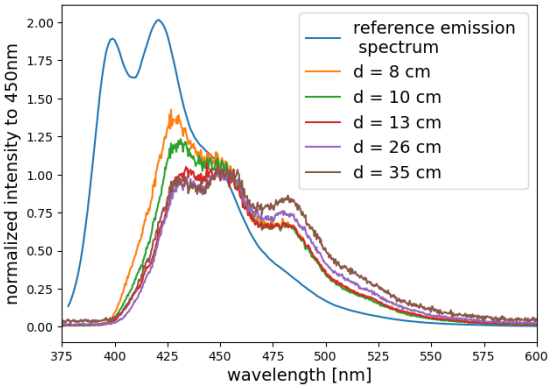

Figure 3: Distance-dependent emission spectrum of a coated borosilicate rod. For the measurement, a borosilicate rod was coated with the wavelength-shifting paint and illuminated with a UV lamp. The spectrum was measured at one end of the tube depending on the distance of the illumination point to the observed end. The reference was measured with a coated cuvette in a flourospectrometer.

the spectrum are cut off.
Therefore, the thickness of the coating has to be weighed against the capture rate and light propagation properties.

2.2 Timing and Attenuation

Contrary to the DOMs and other IceCube Upgrade modules the main contribution for the timing delay of the WOM comes not from the PMTs, but the propagation of the photons inside the tube. Therefore, studying the timing is necessary to infer fundamental detector properties needed for a proper analysis as well as to determine important loss factors of our module like the attenuation inside the tube.

The setup for the timing measurement is shown in Figure 4. The distribution of the arrival times of the photons from this measurement includes

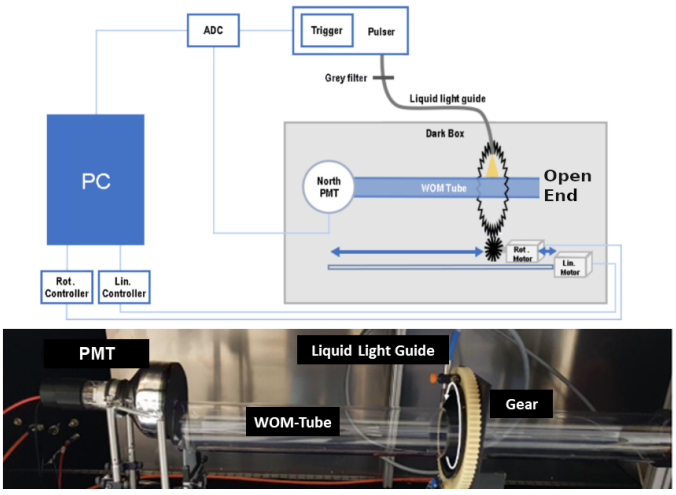

Figure 4: Setup for the timing measurement using a coated PMMA tube. A pico-second pulser [11] is used as the light source. The tube is coupled to the PMT using optical gel. Due to the open end on the right side of the tube half of the photons take a much longer way through the tube, because of the reflection at the open end. This results in a smaller second peak in the timing distribution.

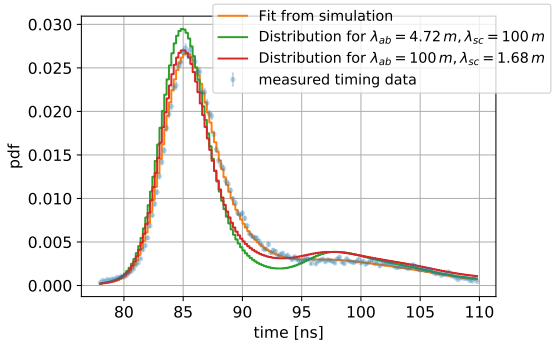

Figure 5: Timing distribution fit at an illumination distance of d=8 cm. $\lambda_{ab} = 4.72\,\text{m}, \lambda_{sc} = 1.68\,\text{m}$. We fit our measured timing data to our model, which results from a convolution of the four described contributions, with the absorption λ_{ab} and scattering length λ_{sc} as free parameters. We can also see the sensitivity of the curve on λ_{ab} and λ_{sc} by comparing the fitted distribution with distributions of other absorbtion and scattering lengths.

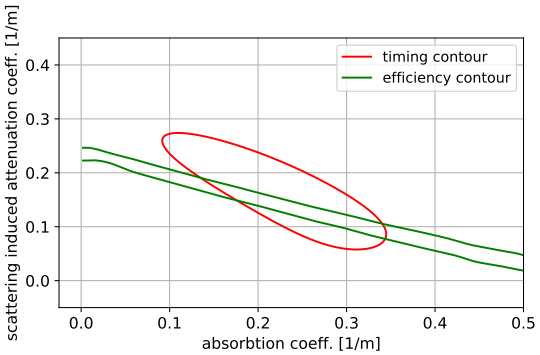

Figure 6: Combined timing and efficiency fit. The efficiency of the WOM is measured with a different setup explained in [9], also while the other end of the tube is open. For the efficiency we get a value for every distance and $\lambda_{ab}, \lambda_{sc}$ combination from the simulation which we fit to the data. Here the efficiencies for every distance combine into one fit.

several different contributions.
The photon propagation inside the tube was modeled by a ray-tracing simulation with adjustable tube geometry and absorption and scattering lengths [12]. The absorption and scattering lengths will be then used as free parameters to fit our timing measurements to a model containing all contributions explained here. Combining these two fitting parameters, the attenuation length of the coated tube can be determined.
The timing distribution of the WLS-paint layer was measured and fitted to follow an exponential distribution $P(t) \sim e^{-\frac{t}{\tau}}$ with $\tau \approx 1.6\,\text{ns}$ [9].
The PMT transit time spread was measured beforehand to be $\sigma \approx 1.5\,\text{ns}$ by illuminating the PMT vertically with the light source. Further, having a relatively flat angular distribution at the exit of the tube one expects an additional widening in the measured timing distribution. This effect is considered by convoluting the previous effect with a Gaussian, where σ is a nuisance parameter in our fit.

Fitting the simulation to the measured timing distribution (see Figure 5) we observe a good data agreement concluding one can describe the observed WOM timing by the four effects mentioned above. Further, we can see the the second timing peak at around 98 ns from the open end reflection mentioned above which can be clearly separated from the first peak. The position and height of this second peak depends on the distance and attenuation length which increases our fit sensitivity to the attenuation length as seen by comparing the three curves from Figure 5.

To determine the attenuation of the coated tube we sum up all likelihoods from the fits at different distances and perform a combined fit and creating a χ^2- sensitivity map giving us an error-contour for the resulting $\lambda_{ab}, \lambda_{sc}$ combination. The same can be also done for the efficiency

measurements of the tube, resulting in two combined error contours we can overlap to constrain the error on the attenuation length (see Figure 6). The attenuation length for the coated tube from both combined fits therefore is

$$\lambda_{att} = 2.65^{+0.38}_{-0.36}\,\mathrm{m}. \tag{2}$$

This value is also compatible with $\lambda_{att} = 3\,\mathrm{m}$ from the efficiency fit to an analytical model done in [9].

From the timing measurements it is now possible to characterize the timing spread of the WOM considering significant systematics. Also, we can disentangle the absorption and scattering and determine the attenuation length of the coated tubes.

3. Application for the IceCube Upgrade

3.1 Dark Noise Rate

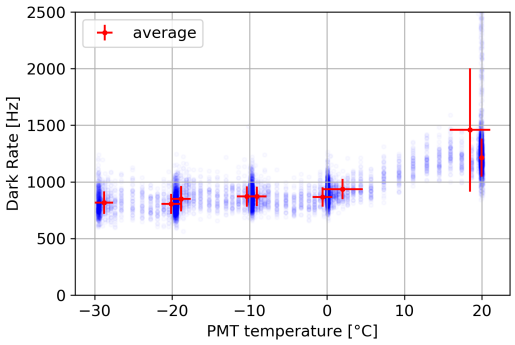

Figure 7: WOM PMT Dark Noise Measurement. Taken at 10^7 gain. We get an average dark noise rate of 800 Hz per PMT at −20 °C which is approximately the ice temperature expected in IceCube.

One big advantage of the WOM mentioned above is the low noise rate which results from the low noise quartz glass and a considerably small PMT area. The quartz glass gives us a contribution of ∼ 60 Hz [9] to the overall noise rate of the module which is negligible compared to the dark noise rate of the two 5" ET9390B PMTs [8] used for the WOM. The PMT dark noise rate was measured at a gain of 10^7 while temperature cycling down to −30 °C. The temperature dependent noise rate can be seen in Figure 7. The measurements result in an average noise rate of 800 Hz per PMT at temperatures expected at the depths where IceCube has instrumented sensors giving the WOM an overall noise rate of ∼ 1600 Hz. This is almost ten times lower than the mDOM noise rate of ∼ 15 kHz (consisting of 24 PMTs with noise rates of 400 − 700 Hz) [13]. The WOM has an effective area of ∼ 20 cm^2 in a wavelength range of 250 − 400 nm [9] while it is ∼ 100 cm^2 at 300 − 600 nm for the mDOM [13]. Considering the small spacing between modules and the low event distance for low-energy events its UV-sensitivity makes the WOM a favorable module for this scenario.

3.2 Upgrade WOM Prototype

The WOM design for the IceCube Upgrade has advanced to the production of the first optomechanical prototype. Multiple WLS coated tubes have been produced. We characterize the tube by determining the attenuation length of light travelling inside the tube λ_{att} and a distance-independent loss factor at interfaces N (see Figure 9), the efficiency as a function of the wavelength (see Figure 8) and the homogeneity of the WLS-paint layer as a function of the z coordinate and the symmetry angle ϕ around the tube (see Figure 10).

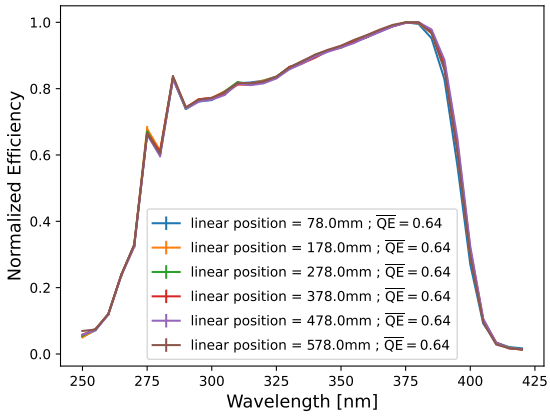

Figure 8: Normalized efficiency as a function of the wavelength for different z positions on the Tube. The quantum efficiency, averaged over the wavelength range $\overline{\text{QE}}$ is is shown for each distance.

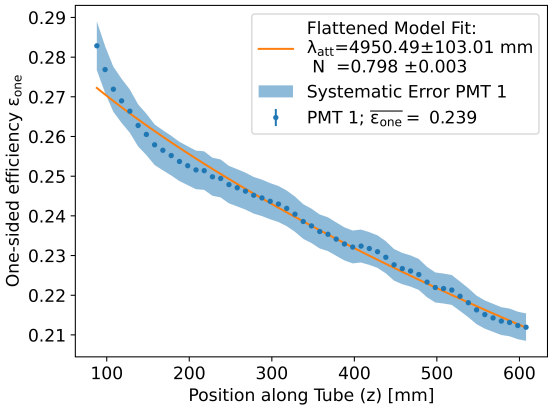

Figure 9: Attenuation length λ_{att} and constant loss factor N extracted from fitting to the distance dependent one sided efficiency $\epsilon_{\text{one}}(z)$. A detailed explanation of the fit function is given in [9].

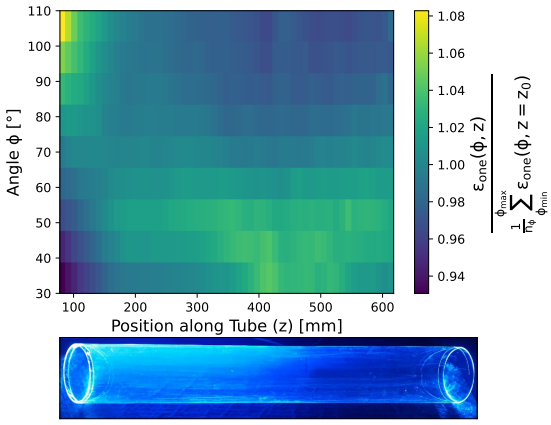

Figure 10: Paint homogeneity measurement. The colorbar compares the one sided efficiency ($\epsilon_{\text{one}}(\phi, z)$) to the mean efficiency value $\epsilon_{\text{one}}(\phi, z = z_0)$ over all ϕ values at z_0. The UV illuminated inner tube is shown at the bottom.

We report an attenuation length in the light collector of $\sim$ 5 m, a normalization constant of $N = 0.8$, an average quantum efficiency of 64 % and a homogeneity over the tube's surface of ±7 %.

4. Wavelength-shifting for IceCube Gen2

For IceCube-Gen2 new sensor designs based on wavelength-shifting technology are envisaged. One design features a WLS-coated tube similar to the WOM, but without pressure vessel, photosensors and electronics. These would be coupled to an IceCube-Gen2 segmented sensor [6] for read-out of the collected photons. This device would effectively work as a photon collector trapping photons and guiding them towards existing photosensors planned for IceCube-Gen2. This design offers an economic extension to increase the effective volume of the IceCube-Gen2 detector to low-energetic CCSNe neutrinos.

The use of wavelength-shifting technology is particularly beneficial for detailed studies of the supernova light curve of nearby objects which contain information on the underlying hydrodynamics and other fundamental processes that drive CCSNe. One such features is the Standing Accretion Shock Instability (SASI), which is thought to arise from the sloshing of the material in and out of the neutrino emission region within the supernova. The SASI would result in periodic variations of the CCSNe light curve [14]. IceCube already has sensitivity to these features up to the centre of the Milky Way for the most optimistic models. The use of wavelength shifters has the potential to

extend the observation horizon further out and for less optimistic scenarios to enhance the supernova light curve.

5. Other Applications

The first working prototype of the WOM-concept was deployed at a depth of 2549 m in the Canadian sea for the STRAW-b experiment [15]. While featuring the same wavelength-shifting concept as the IceCube Upgrade WOM it differed in the proportions and components used [16]. The STRAW-b WOM was able to operate stably and provided data of the local bio-luminescence.

Another modified version of the WOM will be used in the envisioned SHiP-experiment [17]. The WOMs are deployed in a liquid scintillator to implement a veto-mechanism in the search for very weakly interacting long-lived particles.

6. Conclusion

The WOM is an UV-sensitive low noise module with advantages to the IceCube Upgrade. The studies on the WLS-paint allow for a precise modeling of the coating process and the maximum allowed paint thickness. An analysis on the light propagation inside the WOM tube shows disentanglement between the absorption and scattering in the tube and gives us a consistent result of $\lambda_{att} \approx 3$ m for the attenuation length. The UV-sensitivity and low noise rate of the WOM results in possible applications in low-energy analysis while an alternative design of a WLS-module would have high potential in supernovae detection for Gen2.

References

[1] **IceCube** Collaboration *JINST* **12** no. 03, (2017) P03012.
[2] **IceCube** Collaboration *A&A* **532** no. A109, (Nov, 2011) .
[3] **IceCube** Collaboration *PoS* **ICRC2019** (2019) 1031.
[4] **IceCube** Collaboration *PoS* **ICRC2021** (2021) 1070.
[5] **IceCube** Collaboration *JINST* **18** no. 04, (2023) P04014.
[6] **IceCube-Gen2** Collaboration *PoS* **ICRC2023** (these proceedings) 979.
[7] P. A. Čerenkov *Phys. Rev.* **52** (Aug, 1937) 378–379.
[8] ET Enterprises, *130 mm (5") photomultiplier 9390B series data sheet*, 2014.
[9] B. Bastian-Querner *et al. Sensors* **22** no. 4, (2022) .
[10] J. Hümmerich Bachelor's thesis, Johannes Gutenberg-Universität Mainz, 2022.
[11] M. Rongen and M. Schaufel *JINST* **13** no. 06, (2018) P06002.
[12] F. Thomas Master's thesis, Johannes Gutenberg-Universität Mainz, 2019.
[13] M. A. Unland Elorrieta. PhD thesis, Universität Münster, 2023.
[14] I. Tamborra *et al. Physical Review Letters* **111** no. 12, (2013) .
[15] I. C. Rea *et al. PoS* **ICRC2021** (2021) 1092.
[16] M. Bubeck Master's thesis, Johannes Gutenberg-Universität Mainz, 2020.
[17] M. Ehlert *et al. JINST* **14** no. 03, (Mar, 2019) P03021.

Full Author List: IceCube Collaboration

R. Abbasi[17], M. Ackermann[63], J. Adams[18], S. K. Agarwalla[40, 64], J. A. Aguilar[12], M. Ahlers[22], J.M. Alameddine[23], N. M. Amin[44], K. Andeen[42], G. Anton[26], C. Argüelles[14], Y. Ashida[53], S. Athanasiadou[63], S. N. Axani[44], X. Bai[50], A. Balagopal V.[40], M. Baricevic[40], S. W. Barwick[30], V. Basu[40], R. Bay[8], J. J. Beatty[20, 21], J. Becker Tjus[11, 65], J. Beise[61], C. Bellenghi[27], C. Benning[1], S. BenZvi[52], D. Berley[19], E. Bernardini[48], D. Z. Besson[36], E. Blaufuss[19], S. Blot[63], F. Bontempo[31], J. Y. Book[14], C. Boscolo Meneguolo[48], S. Böser[41], O. Botner[61], J. Böttcher[1], E. Bourbeau[22], J. Braun[40], B. Brinson[6], J. Brostean-Kaiser[63], R. T. Burley[2], R. S. Busse[43], D. Butterfield[40], M. A. Campana[49], K. Carloni[14], E. G. Carnie-Bronca[2], S. Chattopadhyay[40, 64], N. Chau[12], C. Chen[6], Z. Chen[55], D. Chirkin[40], S. Choi[56], B. A. Clark[19], L. Classen[43], A. Coleman[61], G. H. Collin[15], A. Connolly[20, 21], J. M. Conrad[15], P. Coppin[13], P. Correa[13], D. F. Cowen[59, 60], P. Dave[6], C. De Clercq[13], J. J. DeLaunay[58], D. Delgado[14], S. Deng[1], K. Deoskar[54], A. Desai[40], P. Desiati[40], K. D. de Vries[13], G. de Wasseige[37], T. DeYoung[24], A. Diaz[15], J. C. Díaz-Vélez[40], M. Dittmer[43], A. Domi[26], H. Dujmovic[40], M. A. DuVernois[40], T. Ehrhardt[41], P. Eller[27], E. Ellinger[62], S. El Mentawi[1], D. Elsässer[23], R. Engel[31, 32], H. Erpenbeck[40], J. Evans[19], P. A. Evenson[44], K. L. Fan[19], K. Fang[40], K. Farrag[16], A. R. Fazely[7], A. Fedynitch[57], N. Feigl[10], S. Fiedlschuster[26], C. Finley[54], L. Fischer[63], D. Fox[59], A. Franckowiak[11], A. Fritz[41], P. Fürst[1], J. Gallagher[39], E. Ganster[1], A. Garcia[14], L. Gerhardt[9], A. Ghadimi[58], C. Glaser[61], T. Glauch[27], T. Glüsenkamp[26, 61], N. Goehlke[32], J. G. Gonzalez[44], S. Goswami[58], D. Grant[24], S. J. Gray[19], O. Gries[1], S. Griffin[40], S. Griswold[52], K. M. Groth[22], C. Günther[1], P. Gutjahr[23], C. Haack[26], A. Hallgren[61], R. Halliday[24], L. Halve[1], F. Halzen[40], H. Hamdaoui[55], M. Ha Minh[27], K. Hanson[40], J. Hardin[15], A. A. Harnisch[24], P. Hatch[33], A. Haungs[31], K. Helbing[62], J. Hellrung[11], F. Henningsen[27], L. Heuermann[1], N. Heyer[61], S. Hickford[62], A. Hidvegi[54], C. Hill[16], G. C. Hill[2], K. D. Hoffman[19], S. Hori[40], K. Hoshina[40, 66], W. Hou[31], T. Huber[31], K. Hultqvist[54], M. Hünnefeld[23], R. Hussain[40], K. Hymon[23], S. In[56], A. Ishihara[16], M. Jacquart[40], O. Janik[1], M. Jansson[54], G. S. Japaridze[5], M. Jeong[56], M. Jin[14], B. J. P. Jones[4], D. Kang[31], W. Kang[56], X. Kang[49], A. Kappes[43], D. Kappesser[41], L. Kardum[23], T. Karg[63], M. Karl[27], A. Karle[40], U. Katz[26], M. Kauer[40], J. L. Kelley[40], A. Khatee Zathul[40], A. Kheirandish[34, 35], J. Kiryluk[55], S. R. Klein[8, 9], A. Kochocki[24], R. Koirala[44], H. Kolanoski[10], T. Kontrimas[27], L. Köpke[41], C. Kopper[26], D. J. Koskinen[22], P. Koundal[31], M. Kovacevich[49], M. Kowalski[10, 63], T. Kozynets[22], J. Krishnamoorthi[40, 64], K. Kruiswijk[37], E. Krupczak[24], A. Kumar[63], E. Kun[11], N. Kurahashi[49], N. Lad[63], C. Lagunas Gualda[63], M. Lamoureux[37], M. J. Larson[19], S. Latseva[1], F. Lauber[62], J. P. Lazar[14, 40], J. W. Lee[56], K. Leonard DeHolton[60], A. Leszczyńska[44], M. Lincetto[11], Q. R. Liu[40], M. Liubarska[25], E. Lohfink[41], C. Love[49], C. J. Lozano Mariscal[43], L. Lu[40], F. Lucarelli[28], W. Luszczak[20, 21], Y. Lyu[8, 9], J. Madsen[40], K. B. M. Mahn[24], Y. Makino[40], E. Manao[27], S. Mancina[40, 48], W. Marie Sainte[40], I. C. Mariş[12], S. Marka[46], Z. Marka[46], M. Marsee[58], I. Martinez-Soler[14], R. Maruyama[45], F. Mayhew[24], T. McElroy[25], F. McNally[38], J. V. Mead[22], K. Meagher[40], S. Mechbal[63], A. Medina[21], M. Meier[16], Y. Merckx[13], L. Merten[11], J. Micallef[24], J. Mitchell[7], T. Montaruli[28], R. W. Moore[25], Y. Morii[16], R. Morse[40], M. Moulai[40], T. Mukherjee[31], R. Naab[63], R. Nagai[16], M. Nakos[40], U. Naumann[62], J. Necker[63], A. Negi[4], M. Neumann[43], H. Niederhausen[24], M. U. Nisa[24], A. Noell[1], A. Novikov[44], S. C. Nowicki[24], A. Obertacke Pollmann[16], V. O'Dell[40], M. Oehler[31], B. Oeyen[29], A. Olivas[19], R. Ørsøe[27], J. Osborn[40], E. O'Sullivan[61], H. Pandya[44], N. Park[33], G. K. Parker[4], E. N. Paudel[44], L. Paul[42, 50], C. Pérez de los Heros[61], J. Peterson[40], S. Philippen[1], A. Pizzuto[40], M. Plum[50], A. Pontén[61], Y. Popovych[41], M. Prado Rodriguez[40], B. Pries[24], R. Procter-Murphy[19], G. T. Przybylski[9], C. Raab[37], J. Rack-Helleis[41], K. Rawlins[3], Z. Rechav[40], A. Rehman[44], P. Reichherzer[11], G. Renzi[12], E. Resconi[27], S. Reusch[63], W. Rhode[23], B. Riedel[40], A. Rifaie[1], E. J. Roberts[2], S. Robertson[8, 9], S. Rodan[56], G. Roellinghoff[56], M. Rongen[26], C. Rott[53, 56], T. Ruhe[23], L. Ruohan[27], D. Ryckbosch[29], I. Safa[14, 40], J. Saffer[32], D. Salazar-Gallegos[24], P. Sampathkumar[31], S. E. Sanchez Herrera[24], A. Sandrock[62], M. Santander[58], S. Sarkar[25], S. Sarkar[47], J. Savelberg[1], P. Savina[40], M. Schaufel[1], H. Schieler[31], S. Schindler[26], L. Schlickmann[1], B. Schlüter[43], F. Schlüter[12], N. Schmeisser[62], T. Schmidt[19], J. Schneider[26], F. G. Schröder[31, 44], L. Schumacher[26], G. Schwefer[1], S. Sclafani[19], D. Seckel[44], M. Seikh[36], S. Seunarine[51], R. Shah[49], A. Sharma[61], S. Shefali[32], N. Shimizu[16], M. Silva[40], B. Skrzypek[14], B. Smithers[4], R. Snihur[40], J. Soedingrekso[23], A. Søgaard[22], D. Soldin[32], P. Soldin[1], G. Sommani[11], C. Spannfellner[27], G. M. Spiczak[51], C. Spiering[63], M. Stamatikos[21], T. Stanev[44], T. Stezelberger[9], T. Stürwald[62], T. Stuttard[22], G. W. Sullivan[19], I. Taboada[6], S. Ter-Antonyan[7], M. Thiesmeyer[1], W. G. Thompson[14], J. Thwaites[40], S. Tilav[44], K. Tollefson[24], C. Tönnis[56], S. Toscano[12], D. Tosi[40], A. Trettin[63], C. F. Tung[6], R. Turcotte[31], J. P. Twagirayezu[24], B. Ty[40], M. A. Unland Elorrieta[43], A. K. Upadhyay[40, 64], K. Upshaw[7], N. Valtonen-Mattila[61], J. Vandenbroucke[40], N. van Eijndhoven[13], D. Vannerom[15], J. van Santen[63], J. Vara[43], J. Veitch-Michaelis[40], M. Venugopal[31], M. Vereecken[37], S. Verpoest[44], D. Veske[46], A. Vijai[19], C. Walck[54], C. Weaver[24], P. Weigel[15], A. Weindl[31], J. Weldert[60], C. Wendt[40], J. Werthebach[23], M. Weyrauch[31], N. Whitehorn[24], C. H. Wiebusch[1], N. Willey[24], D. R. Williams[58], L. Witthaus[23], A. Wolf[1], M. Wolf[27], G. Wrede[26], X. W. Xu[7], J. P. Yanez[25], E. Yildizci[40], S. Yoshida[16], R. Young[36], F. Yu[14], S. Yu[24], T. Yuan[40], Z. Zhang[55], P. Zhelnin[14], M. Zimmerman[40]

[1] III. Physikalisches Institut, RWTH Aachen University, D-52056 Aachen, Germany
[2] Department of Physics, University of Adelaide, Adelaide, 5005, Australia
[3] Dept. of Physics and Astronomy, University of Alaska Anchorage, 3211 Providence Dr., Anchorage, AK 99508, USA
[4] Dept. of Physics, University of Texas at Arlington, 502 Yates St., Science Hall Rm 108, Box 19059, Arlington, TX 76019, USA
[5] CTSPS, Clark-Atlanta University, Atlanta, GA 30314, USA
[6] School of Physics and Center for Relativistic Astrophysics, Georgia Institute of Technology, Atlanta, GA 30332, USA
[7] Dept. of Physics, Southern University, Baton Rouge, LA 70813, USA
[8] Dept. of Physics, University of California, Berkeley, CA 94720, USA
[9] Lawrence Berkeley National Laboratory, Berkeley, CA 94720, USA
[10] Institut für Physik, Humboldt-Universität zu Berlin, D-12489 Berlin, Germany
[11] Fakultät für Physik & Astronomie, Ruhr-Universität Bochum, D-44780 Bochum, Germany
[12] Université Libre de Bruxelles, Science Faculty CP230, B-1050 Brussels, Belgium

[13] Vrije Universiteit Brussel (VUB), Dienst ELEM, B-1050 Brussels, Belgium
[14] Department of Physics and Laboratory for Particle Physics and Cosmology, Harvard University, Cambridge, MA 02138, USA
[15] Dept. of Physics, Massachusetts Institute of Technology, Cambridge, MA 02139, USA
[16] Dept. of Physics and The International Center for Hadron Astrophysics, Chiba University, Chiba 263-8522, Japan
[17] Department of Physics, Loyola University Chicago, Chicago, IL 60660, USA
[18] Dept. of Physics and Astronomy, University of Canterbury, Private Bag 4800, Christchurch, New Zealand
[19] Dept. of Physics, University of Maryland, College Park, MD 20742, USA
[20] Dept. of Astronomy, Ohio State University, Columbus, OH 43210, USA
[21] Dept. of Physics and Center for Cosmology and Astro-Particle Physics, Ohio State University, Columbus, OH 43210, USA
[22] Niels Bohr Institute, University of Copenhagen, DK-2100 Copenhagen, Denmark
[23] Dept. of Physics, TU Dortmund University, D-44221 Dortmund, Germany
[24] Dept. of Physics and Astronomy, Michigan State University, East Lansing, MI 48824, USA
[25] Dept. of Physics, University of Alberta, Edmonton, Alberta, Canada T6G 2E1
[26] Erlangen Centre for Astroparticle Physics, Friedrich-Alexander-Universität Erlangen-Nürnberg, D-91058 Erlangen, Germany
[27] Technical University of Munich, TUM School of Natural Sciences, Department of Physics, D-85748 Garching bei München, Germany
[28] Département de physique nucléaire et corpusculaire, Université de Genève, CH-1211 Genève, Switzerland
[29] Dept. of Physics and Astronomy, University of Gent, B-9000 Gent, Belgium
[30] Dept. of Physics and Astronomy, University of California, Irvine, CA 92697, USA
[31] Karlsruhe Institute of Technology, Institute for Astroparticle Physics, D-76021 Karlsruhe, Germany
[32] Karlsruhe Institute of Technology, Institute of Experimental Particle Physics, D-76021 Karlsruhe, Germany
[33] Dept. of Physics, Engineering Physics, and Astronomy, Queen's University, Kingston, ON K7L 3N6, Canada
[34] Department of Physics & Astronomy, University of Nevada, Las Vegas, NV, 89154, USA
[35] Nevada Center for Astrophysics, University of Nevada, Las Vegas, NV 89154, USA
[36] Dept. of Physics and Astronomy, University of Kansas, Lawrence, KS 66045, USA
[37] Centre for Cosmology, Particle Physics and Phenomenology - CP3, Université catholique de Louvain, Louvain-la-Neuve, Belgium
[38] Department of Physics, Mercer University, Macon, GA 31207-0001, USA
[39] Dept. of Astronomy, University of Wisconsin–Madison, Madison, WI 53706, USA
[40] Dept. of Physics and Wisconsin IceCube Particle Astrophysics Center, University of Wisconsin–Madison, Madison, WI 53706, USA
[41] Institute of Physics, University of Mainz, Staudinger Weg 7, D-55099 Mainz, Germany
[42] Department of Physics, Marquette University, Milwaukee, WI, 53201, USA
[43] Institut für Kernphysik, Westfälische Wilhelms-Universität Münster, D-48149 Münster, Germany
[44] Bartol Research Institute and Dept. of Physics and Astronomy, University of Delaware, Newark, DE 19716, USA
[45] Dept. of Physics, Yale University, New Haven, CT 06520, USA
[46] Columbia Astrophysics and Nevis Laboratories, Columbia University, New York, NY 10027, USA
[47] Dept. of Physics, University of Oxford, Parks Road, Oxford OX1 3PU, United Kingdom
[48] Dipartimento di Fisica e Astronomia Galileo Galilei, Università Degli Studi di Padova, 35122 Padova PD, Italy
[49] Dept. of Physics, Drexel University, 3141 Chestnut Street, Philadelphia, PA 19104, USA
[50] Physics Department, South Dakota School of Mines and Technology, Rapid City, SD 57701, USA
[51] Dept. of Physics, University of Wisconsin, River Falls, WI 54022, USA
[52] Dept. of Physics and Astronomy, University of Rochester, Rochester, NY 14627, USA
[53] Department of Physics and Astronomy, University of Utah, Salt Lake City, UT 84112, USA
[54] Oskar Klein Centre and Dept. of Physics, Stockholm University, SE-10691 Stockholm, Sweden
[55] Dept. of Physics and Astronomy, Stony Brook University, Stony Brook, NY 11794-3800, USA
[56] Dept. of Physics, Sungkyunkwan University, Suwon 16419, Korea
[57] Institute of Physics, Academia Sinica, Taipei, 11529, Taiwan
[58] Dept. of Physics and Astronomy, University of Alabama, Tuscaloosa, AL 35487, USA
[59] Dept. of Astronomy and Astrophysics, Pennsylvania State University, University Park, PA 16802, USA
[60] Dept. of Physics, Pennsylvania State University, University Park, PA 16802, USA
[61] Dept. of Physics and Astronomy, Uppsala University, Box 516, S-75120 Uppsala, Sweden
[62] Dept. of Physics, University of Wuppertal, D-42119 Wuppertal, Germany
[63] Deutsches Elektronen-Synchrotron DESY, Platanenallee 6, 15738 Zeuthen, Germany
[64] Institute of Physics, Sachivalaya Marg, Sainik School Post, Bhubaneswar 751005, India
[65] Department of Space, Earth and Environment, Chalmers University of Technology, 412 96 Gothenburg, Sweden
[66] Earthquake Research Institute, University of Tokyo, Bunkyo, Tokyo 113-0032, Japan

Acknowledgements

The authors gratefully acknowledge the support from the following agencies and institutions: USA – U.S. National Science Foundation-Office of Polar Programs, U.S. National Science Foundation-Physics Division, U.S. National Science Foundation-EPSCoR, Wisconsin Alumni Research Foundation, Center for High Throughput Computing (CHTC) at the University of Wisconsin–Madison, Open Science

Grid (OSG), Advanced Cyberinfrastructure Coordination Ecosystem: Services & Support (ACCESS), Frontera computing project at the Texas Advanced Computing Center, U.S. Department of Energy-National Energy Research Scientific Computing Center, Particle astrophysics research computing center at the University of Maryland, Institute for Cyber-Enabled Research at Michigan State University, and Astroparticle physics computational facility at Marquette University; Belgium – Funds for Scientific Research (FRS-FNRS and FWO), FWO Odysseus and Big Science programmes, and Belgian Federal Science Policy Office (Belspo); Germany – Bundesministerium für Bildung und Forschung (BMBF), Deutsche Forschungsgemeinschaft (DFG), Helmholtz Alliance for Astroparticle Physics (HAP), Initiative and Networking Fund of the Helmholtz Association, Deutsches Elektronen Synchrotron (DESY), and High Performance Computing cluster of the RWTH Aachen; Sweden – Swedish Research Council, Swedish Polar Research Secretariat, Swedish National Infrastructure for Computing (SNIC), and Knut and Alice Wallenberg Foundation; European Union – EGI Advanced Computing for research; Australia – Australian Research Council; Canada – Natural Sciences and Engineering Research Council of Canada, Calcul Québec, Compute Ontario, Canada Foundation for Innovation, WestGrid, and Compute Canada; Denmark – Villum Fonden, Carlsberg Foundation, and European Commission; New Zealand – Marsden Fund; Japan – Japan Society for Promotion of Science (JSPS) and Institute for Global Prominent Research (IGPR) of Chiba University; Korea – National Research Foundation of Korea (NRF); Switzerland – Swiss National Science Foundation (SNSF); United Kingdom – Department of Physics, University of Oxford.